

Effects of Leading Edge Enlargement on the Primary Vortex of Blunt-Edged Delta Wing VFE-2 Profile

Mazuriah Said, Shabudin Mat, Shuhaimi Mansor and Airi Ali

Department of Aeronautics, Automotive and Ocean Engineering, School of Mechanical Engineering, Faculty of Engineering, Universiti Teknologi Malaysia, 81310 Skudai, Johor, Malaysia

mazuriah2@graduate.utm.my, shabudin@fkm.utm.my,
shuhaimi@mail.fkm.utm.my, airi.ali@utm.my

Abstract: This paper presents the results obtained from wind tunnel experiments on VFE-2 wing profile model which are differentiated by their leading edge profiles; medium- and large-edged. VFE-2 was established to investigate the effects of Reynolds number, angle of attack, Mach number and leading edge bluntness on vortex properties above-blunt-edged delta wing. The original VFE-2 wing has 4 sets of interchangeable leading edge profile namely sharp, small, medium and large-edge ratio. There were lot of experiments and simulations data in VFE that compares sharp-edged with the medium-edged wings within the VFE campaign. This paper presents the current data on a blunter wing or large-edged wing. These experiments were conducted at UTM - Low Speed Wind Tunnel, Aerolab. The experiments were carried out at speed of 18, 36 and 54 m/s representing Reynolds numbers of 1×10^6 , 2×10^6 & 3×10^6 . Two measurement techniques were employed on the wing, i.e. steady balance and surface pressure measurements. The results obtained from the large-edged wing were compared with the results from medium-edge wing. The results showed that the primary vortex depends on the leading edge bluntness, angle of attack and Reynolds number. The results obtained from steady balance data showed that lift coefficient is sensitive to leading edge bluntness at higher Reynolds numbers. Several important observations were noted on the large-edged wing; i.e. the development of primary vortex has been delayed and the vortex breakdown occurred further aft of the wing. The data obtained provide a better insight into the leading edge effect on the delta-shaped wing and also for the development of Unmanned Combat Air Vehicle (UCAV) which most of them are integrated with delta wing technology.

Keywords: Delta wing; VFE-2 profile; Vortex; blunt leading edge; Reynolds number

1 Blunt-edged Flow Topology

The exploitation of vortex lift on delta wing existed since 1940's [1]. Since then, there are researches that investigate the vortex flows above sharp-edge delta wing [2-5]. On sharp-edged delta wing; primary separation takes place when a stable shear layer is formed from a series of small vortices that shed in the leading edge of the wing. These shear layers form curling up over the wing upper surface into concentrated vortices in a spiral fashion [2-4]. The *primary vortex* is generated and initiated from the wing apex and it grows in strength and size extended towards the wing trailing edge. Underneath this primary vortex, the adverse pressure gradient increases in the region and another spinning vortex is developed in the leading edge. This vortex is called the *secondary vortex*, which rotates in the opposite direction of the primary vortex. [2].

The flow on blunt-edged delta is different from the flow formed on the sharp-edged delta wing. Firstly, the flow separation does not happen in the apex region. The flow is attached to the surface of the wing in a certain chord-wise position. The primary vortex is then developed further aft of the wing that is based on a Reynolds number, angle of attack and leading-edge bluntness [6-8]. This shows that the onset of leading-edge separation was a function of flow conditions such as Reynolds number, Mach number, blockage factors and wing geometry [9]. Another important flow phenomenon is that the primary separation line no longer occurs at the leading edge but somewhere in vicinity of it [6]. This causes the flow on the blunt-edged wing to be complicated and unpredictable.

Therefore, a research group has been established across Europe and USA to further investigate flow phenomena on a blunt-edged delta wing. This group is called as VFE-2 or International Vortex Flow Experiment 2 under AVT-113. The group has the objective to compare the results obtained from numerical calculations with wind tunnel experiments [9]. This group has used the original Chu and Luckring [10] model tested in NASA NTF shown in Figure 1(a) as a generic profile. The NASA original model has a flat plate in the middle with 4 sets of interchangeable leading edge profiles namely as the sharp-edged, small-edged, medium-edged and large-edged. These leading edge profiles were differentiated by its leading edge radii to the wing chord ratio; i.e. 0 for sharp, 0.05 for small-edged, 0.15 for medium-edged and 0.30 for large-edged wing as shown in Figure 1(b).

During the VFE-2 campaign, only the second wing or medium-edged wing was selected for further experiments in several wind tunnels such as Glasgow University [11-13], Tubitak Sage [14], Munich Technical University [15], ONERA [16] and several other wind tunnel facilities. The main objective of the campaign at that time was to study how either the numerical analysis or CFD can well predict the flow on the blunt-edged delta wing. The results obtained from the wind tunnel experiments were compared with the results obtained from Numerical analysis.

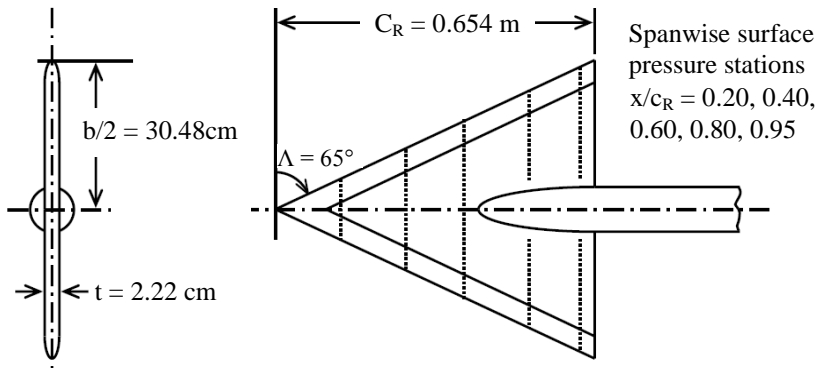


Figure 1(a)

Original NASA and VFE-2 configuration [9]

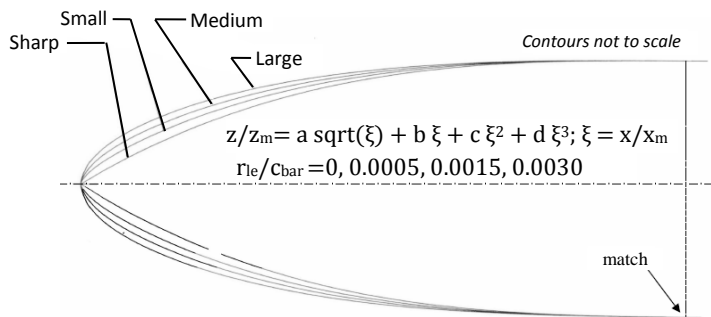


Figure 1(b)

Streamwise leading-edge contours of original NASA and VFE-2 configuration [8]

The sample results taken from VFE-2 [17] campaign of the medium-edged wing are shown in Figure 2 below. The flow on the medium-edge wing is covered by a non-separated flow on the entire wing at a low angle of attack. However, it is unclear whether the vortex is developed further aft of the wing in the trailing edge. No data is available to date [13]. When the attack angle is increased, the primary vortex is formed at a certain chordwise position from the apex as shown in Figure 2 below. From the figure, it can be observed the wing has been covered by two main sections, i.e. the attached flow and the primary vortex. The primary vortex moved forward or backward depending on the angle of attack, the Reynolds number and also the leading edge bluntness. Increasing in angle of attack has caused the primary vortex to move forward; there is no data that can indicate the primary vortex is formed in the apex region if the angle of attack continues to be increased to more than $\alpha = 25^\circ$ to date.

Reduction the Reynolds number has caused the primary vortex to move forward as shown in Figure 2. The comparison here was made between the results at R_{mac}

of 3×10^6 and R_{mac} of 2×10^6 at constant α of 13° and Mach number of 0.4. It cannot be confirm, also, whether the primary vortex will develop in the apex region if the Reynolds number is further decreased. Another factor that influenced the flow is the leading edge bluntness itself; an increase in leading edge bluntness has caused the primary vortex to be delayed. However the data on the blunter wing of large-edged is still limited [8-19]. Another important observation that has been found in the VFE-2 group was that they found another vortex formed inboard of the wing. This vortex is named *inner vortex*. The formation of this vortex also depends on leading edge bluntness, Reynolds number and also the angle of attack. More experiments are necessary to study this vortex at a higher leading-edge radius [13, 15, 17-18, 20].

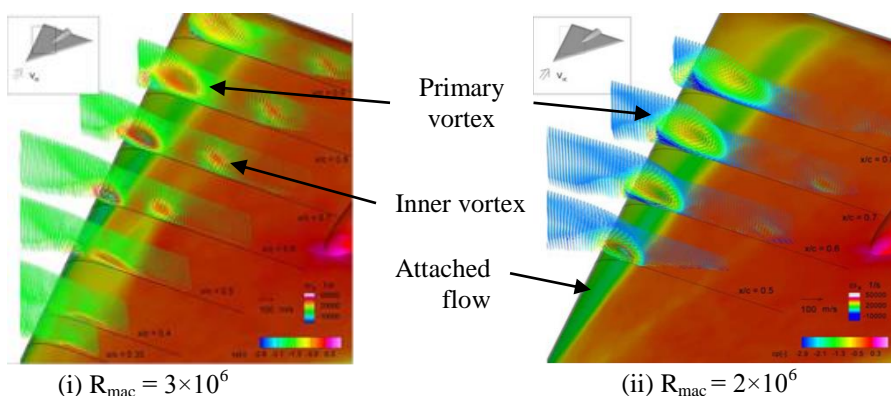


Figure 2

Pressure distributions on VFE-2 configuration at $\alpha = 13^\circ$, $M = 0.4$ on medium-edged wing at (i) R_{mac} of 3×10^6 and (ii) at R_{mac} of 2×10^6 [17]

A research group has been established in UTM to further investigate the influences of leading edge bluntness and Reynolds number on the VFE-2 model. Since the VFE-2 research group has focused on the Medium-edged wing, the team in UTM has decided to focus more on a blunter wing with a large-edged profile. The main purpose of conducting the experiment on the large-edged wing was to further investigate the characteristics of the primary vortex and vortex breakdown at higher leading edge bluntness. In addition, the surface pressure data on this wing is very limited as the VFE-2 group has only focused on the medium-edged wing. In this current paper, the experiments performed at Reynolds number varies from 1×10^6 to 3×10^6 where the flow is strongly influenced by laminar, transition and turbulence. Current data such as drag and detailed surface pressure measurement obtained from the large-edged wing were compared with the medium-edge wing. Therefore, this paper presents the flow characteristics of VFE-2 profile when the leading edge bluntness is increased. Some interesting data will be discussed in the next sub section.

2 Experimental Tests Set-Up

2.1 UTM Aerolab

The experiments were conducted in a closed-circuit UTM-LST wind tunnel facility in Aerolab (refer Figure 5). The dimension of the test section is 2.0 m (W) \times 1.5 m (H) \times 5.8 m (L) with maximum speed of 80 m/s . The average turbulence intensity at the centre of the test section is 0.06% measured at 40 m/s . The boundary layer thickness is about 40 mm at a speed of 40 m/s . The facility was equipped with 3–strut–support system located underneath the test section.

2.2 UTM VFE-2 Model

The original 65° swept angle NASA delta wing model tested in NASA [9] or called as VFE-2 configuration in AVT-113 campaign has been replicated and machined again in UTM under the Malaysian Ministry of Education Research Grant for further experiments at lower Reynolds number. The original NASA model has 4 sets of interchangeable leading edges namely as sharp, small, medium and large radius wing that corresponding to the ratio of leading-edge radii to mean aerodynamics chords r_{LE} of 0, 0.05, 0.15 and 0.3 respectively. In UTM, only two blunter wings, namely medium and large radius wings were built for further experiments. This model is named as UTM VFE-2. The model has a root chord length of, $C_R = 1.311\text{ m}$. The size of the UTM VFE-2 model is 2 times bigger than the original NASA model. This is done in order to get a high Reynolds number ($R_{mac} = 3 \times 10^6$) in a subsonic wind tunnel. The original NASA model was tested in the transonic wind tunnel. The final dimensions of UTM-VFE-2 model and the contours of both leading edges are shown in Figure 3. The UTM VFE-2 model has been machined from three main components. The first component is called a flat-plate delta shaped with fix sharp trailing edge portion. The second components are the leading edges itself, both leading edges will be attached to the flat plate during the experiments. The final component is called as lower surface flat cover. All parts were made from aluminium as shown in Figure 4.

2.3 Measurement Techniques

The experiments were carried out at the Reynolds number of 1×10^6 , 2×10^6 & 3×10^6 corresponding to the speeds of 18 , 36 & 54 m/s base on the mean aerodynamic chord of 0.87 m . The angles of attacks were varied from $0^\circ \leq \alpha \leq 25^\circ$ with 3° increment. The models were attached to six-component external balances located underneath turntable. The models installation is shown in Figure 5. From the figure, the model angle of attack can be created by adjusting the aft support vertically. Two measurements techniques were employed on the model. The first experiment was the steady balance data to obtain the forces and moments in x , y and z . The steady balance data are measured using a heavy capacity external balance located underneath the wind tunnel. This load cell can measure the forces

and moments in 6 axes. For this project, the lift and drag are measured by forces in $-x$ and $-y$ axes while the pitching moment is measured by the moment in the $-z$ axis. The sampling rate for each channels were captured at 100 Hz.

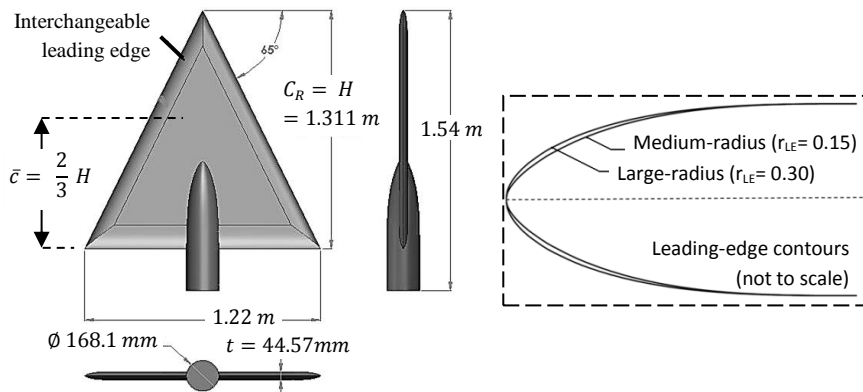


Figure 3
Dimensions of UTM VFE-2 model

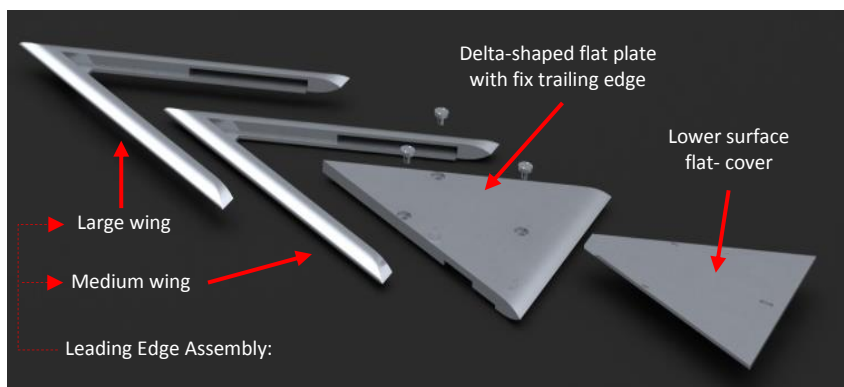


Figure 4
Delta wing model assembly

The final experiment was the surface pressure measurements that were captured on the upper surface of the wing. There were 86 pressure taps located on starboard side of the wing. The diameter of the orifice was $d_{outer} = 1 \text{ mm}$ which located normal to the wing surface. The pressure taps were arranged in 10 different chord-wise stations started from 10% to 97% from the wing apex, i.e. in Y/C_R of 0.1, 0.2, 0.3, 0.4, 0.5, 0.6, 0.7, 0.8 and 0.97 of the wing. In spanwise positions, more pressure taps were placed in the leading edge region. This is done in order to measure the primary vortex that developed in the leading edge. This is shown in Figure 6. During the experiment, the data were captured at 1000 samples in 10 second or the sampling rate was 100 Hz. The installation of UTM-VFE-2 model in the test section of UTM-LST is shown in Figure 5 below.

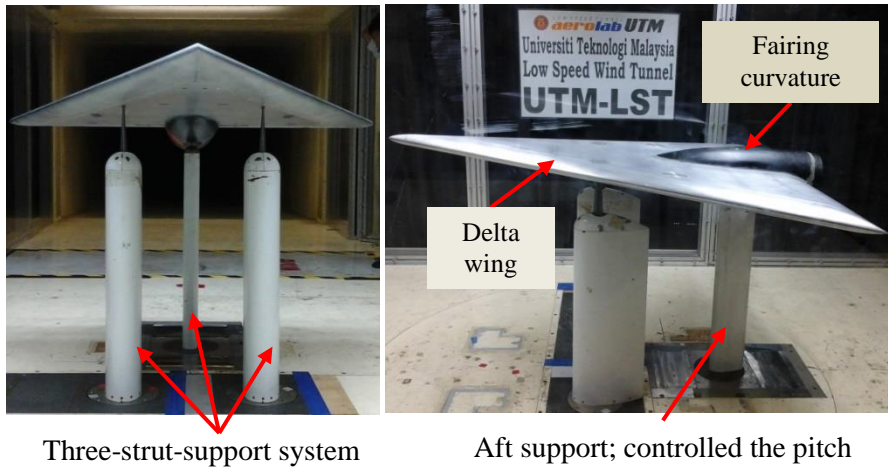
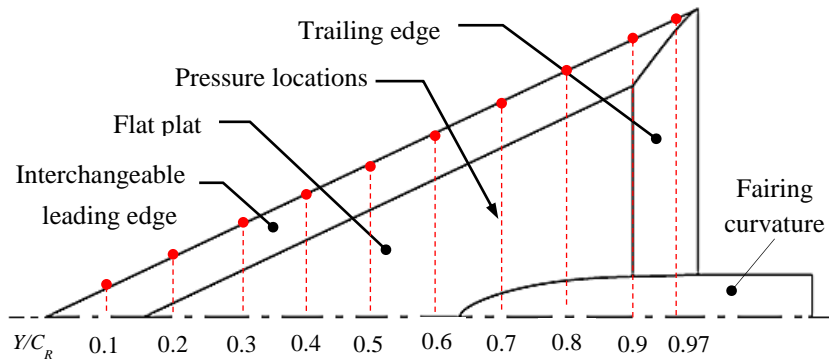


Figure 5
The model installations at UTM-LST



Chord-wise surface pressure locations:
 $Y/C_r = 0.1, 0.2, 0.3, 0.4, 0.5, 0.6, 0.7, 0.8, 0.97$

Figure 6
Leading-edge contours (not to scale)

3 Results and Discussion

In order to observe the impact of leading edge bluntness on the primary vortex, the data obtained from the large-edged wing were compared to the medium-edged wing.

3.1 Medium and Large-edged Flow Characteristics

3.1.1 Aerodynamic Coefficients

The data obtained from the external balance data has been analysed and presented in Figure 7. In order to investigate the influence of leading edge bluntness on C_L , C_D and C_M the data obtained from the large-edged wing has been compared with the results obtained from the medium-edged wing. The sample data at R_{mac} of 3×10^6 is shown in Figure 7 below. The results show that both C_L and C_D are reduced if leading edge bluntness is increased. This is consistent with Mat [12] who experimentally showed that the magnitude of lift and drag forces decrease when the leading edge bluntness is increased. This situation occurs because the strength of the primary vortex is decreasing when leading edge bluntness is increased. The reduction in C_D is also caused by the increase in leading edge suction force acting in the leading edge of the wing.

A clear observation in Figure 7(a) shows that the C_L for large-edged wing reduces compared to medium-edged wing. This situation happened starting from $\alpha = 6^\circ$ onwards. This shows that C_L decreases when the leading edge bluntness is increased. This phenomenon is linked with the strength of the primary vortex. The increases in the leading-edge radius have weakened the primary vortex. The primary vortex is weakened because the primary separation has been delayed by the leading edge profile. Another factor that causes C_L to decrease is the attached flow. The large portion of attached flow covered in the apex region of the large-edged wing has reduces the C_L as shown in Figure 7(a). The large fraction of the leading edge suction force act on the large-edged has contributed to this behaviour and thus increased the C_L/C_D ratio shown in Figure 7(c). The results here consistent with Ronoei [21] who experimentally measured the C_L/C_D ratio on a generic span delta wing.

The pitching moment coefficient (C_M) is plotted in Figure 7(d). In general, both wings show to have a nose-down pitching moment. The medium-edged wing has experienced a higher nose-down C_M compared to the large-edged until $\alpha \approx 13^\circ$. This may link to the greater strength of primary vortex that formed earlier on the medium-edged wing compared to the large-edged wing. At angle of attack $\alpha \geq 13^\circ$, the pitching moment has becomes more negative for both cases. At attack angle higher than $\alpha = 13^\circ$, it is notable that C_M for large-edged wing is higher than medium-edged wing. The reason for this is unknown to date and more experiments are needed to verify this.

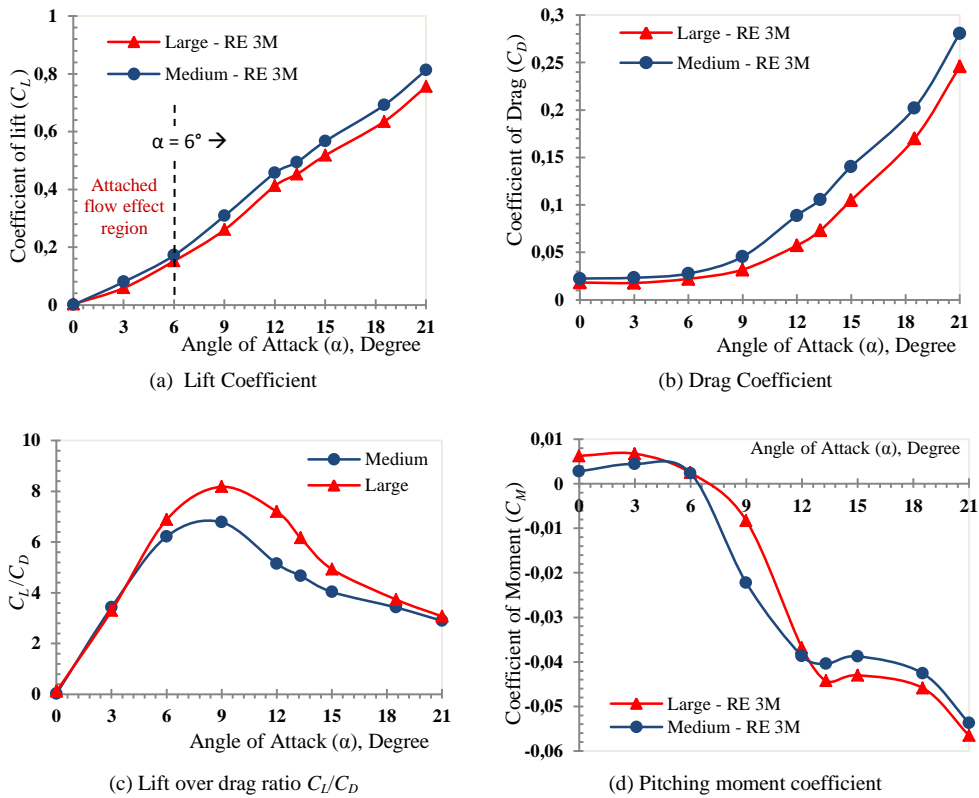


Figure 7
Effects of leading edge bluntness on aerodynamic coefficients at $R_{mac} = 3 \times 10^6$

3.1.2 Surface Pressure Coefficient

This section discusses the results obtained from the surface pressure measurement studies measured on the upper surface of both wings. In order to compare the effects of leading edge bluntness, the surface pressure obtained for large-edged wing has been compared to medium-edged wing. For example, the result at $\alpha = 13^\circ$ and $R_{mac} = 3 \times 10^6$ is compared in Figure 8. The pressure taps were arranged in 10 different chord-wise stations started from 10% to 97% of the wing. For the medium-edged wing, it can be noted that the attached flow is formed from the wing apex to 40% downstream. The primary vortex begins to occur at 50% from the apex. The leading edge effect is obvious here, when the leading edge bluntness is increased, it is notable that the attached flow area on the large-edged has covered about 60% of the wing from the apex. Then, the primary vortex begins at about 70% from the wing apex [19, 22].

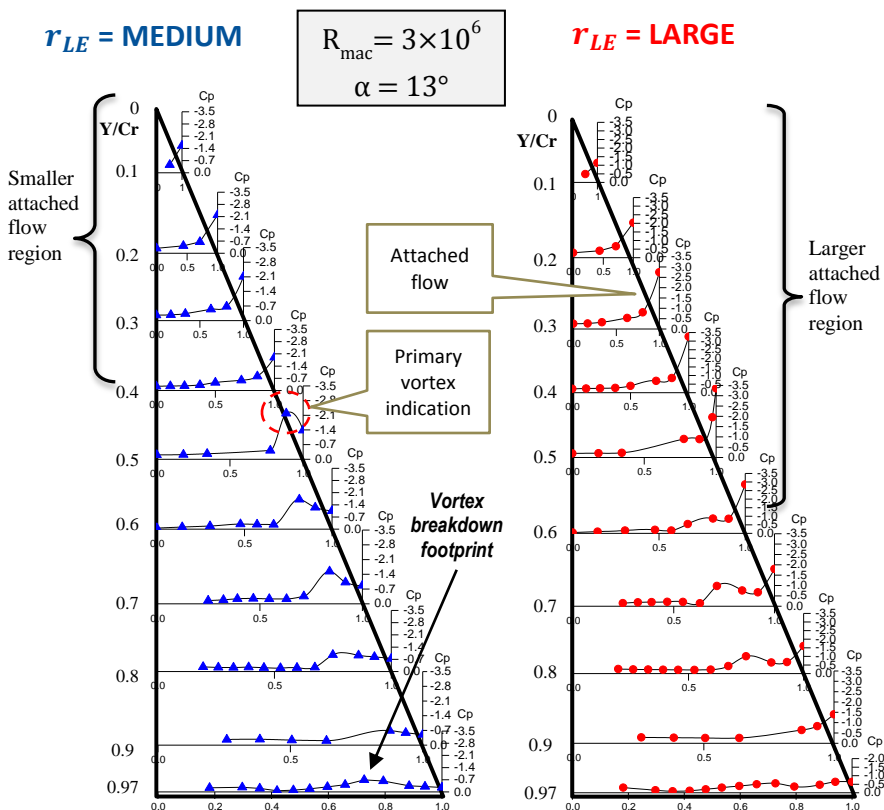


Figure 8

Pressure distribution for Medium- and Large-edged wing at $R_{mac} = 3 \times 10^6$, $\alpha = 13^\circ$

The results at higher angle of attack of $\alpha = 21^\circ$ is shown in Figure 9. The surface pressure for the medium-edged wing has been compared with the data from the large-edged wing in the same figure. From the Figure, it has been noted that the primary vortex has moved forward to 30% from the wing apex on medium-edged wing compared to 40% from the Apex for the large-edged case. This indicates that the upstream progression of the primary vortex has been slowed at a higher angle of attack. In order to observe the strength of the primary vortex on both wings, the pressure coefficient at positions $Y/C_r = 0.3, 0.6 \& 0.7$ were compared in the diagram. From the figure, it can be observed that the peak for the medium-edged wing is relatively higher compared to the large-edged for all positions. This indicates that the strength of the primary vortex decreases if the leading edge bluntness is increased.

The impact of leading edge bluntness on the vortex breakdown is also shown in the figure. A clear observation in the trailing edge area at Y/C_r of 0.8 and below showed that the vortex breakdown is delayed for the large-edged wing compared to the sharper wing of the medium-edged. The stable shear layer on the blunter

wing is suspected to delay the breakdown. By having short run of attached flow in the leading edge region and delay in separation had reduces in the instability of the shear layer on the blunter leading edge [22-23].

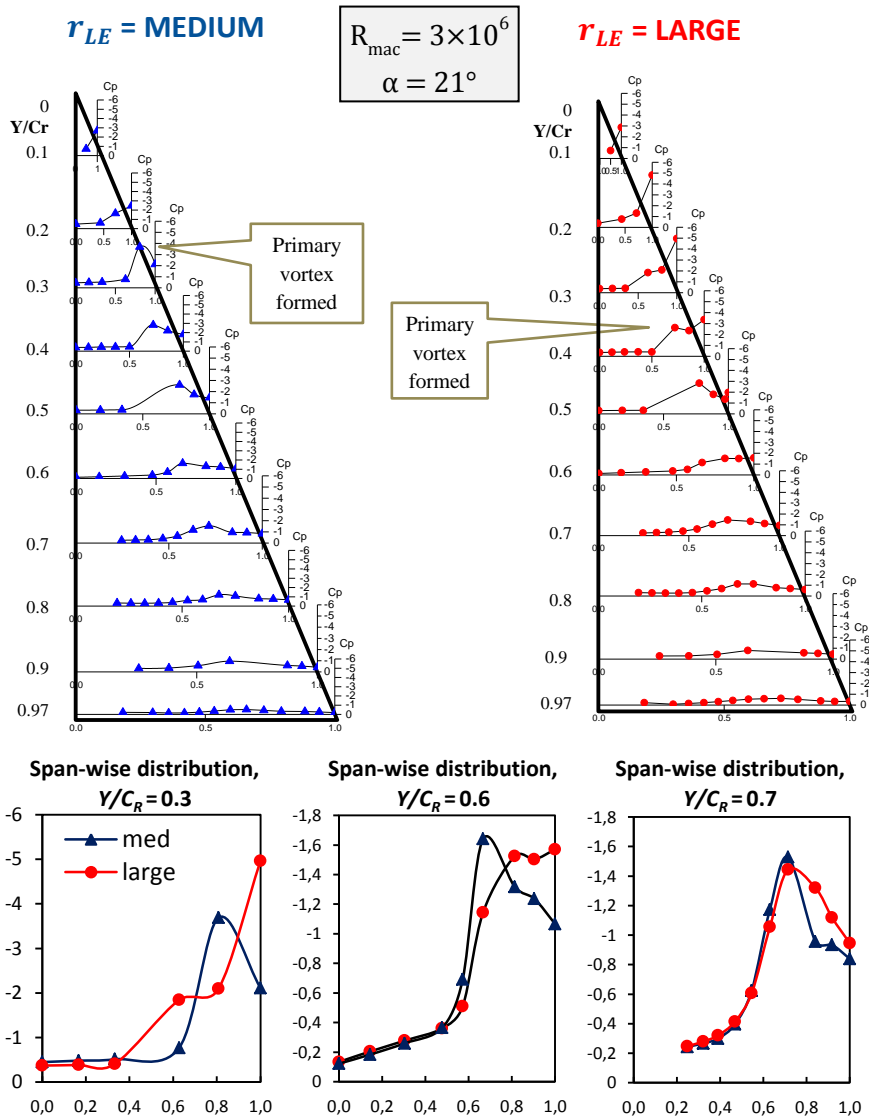


Figure 9
Pressure distribution for Medium- and Large-edged wing at $R_{mac} = 3 \times 10^6$, $\alpha = 21^\circ$

A statistical technique called as Krigging method has been used to obtain the flow topology on the surface of the wing. The sample surface flow topology performed on both wings at $\alpha = 13^\circ$ and R_{mac} of 2×10^6 is shown in Figure 10. The figure shows that the primary vortex is shifted outboard on the blunter wing of the large-edged wing. This again shows that the size and strength of the primary vortex has decreased when the leading edge bluntness is increased.

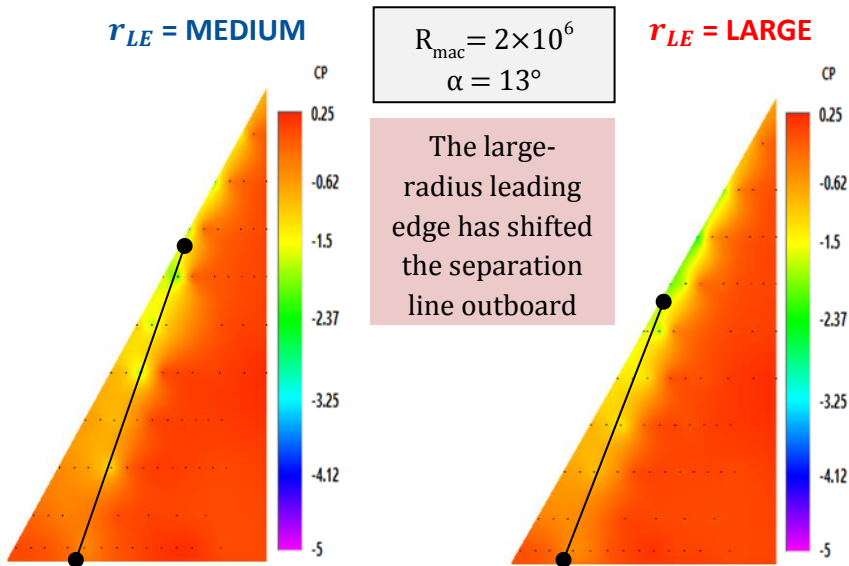


Figure 10

Flow topology comparison at $R_{mac} = 2 \times 10^6$, $\alpha = 13^\circ$

3.1.3 Leading Edge Pressures

The pressure coefficients in the leading edge can be used to predict the onset of the primary vortex on the blunt-edged wing [17-18]. In this case, the leading edge coefficient has been plotted for positions Y/C_r of 0.2, 0.4, 0.5, 0.6 & 0.8 from the apex. This is done in Figure 11 for Reynolds number of 1×10^6 and Figure 12 for Reynolds number of 3×10^6 . At Reynolds number 1×10^6 , the flow remains attached to the surface even at $\alpha = 25^\circ$ for both medium- and large-edged wings at $Y/C_R = 0.2$. The results obtained here contrast with Mat [12-13] who experimentally showed that the primary vortex was developed in the apex area at $R_{mac} = 1 \times 10^6$. An important observation of these current results in the flow is attached to the surface in the apex area as long as the leading edge is blunt [19]. The effects of leading edge bluntness is observed at $Y/C_R = 0.4$ where the flow on the medium-edged wing has separated at $\alpha = 9^\circ$ while it separates at $\alpha = 12^\circ$ for large-edged wing. Similar observation also can be noticed at $Y/C_R = 0.8$ where the separation occurs earlier on the shaper wing. It can be concluded here that the increase in leading bluntness has delayed the formation of vortex above the wing.

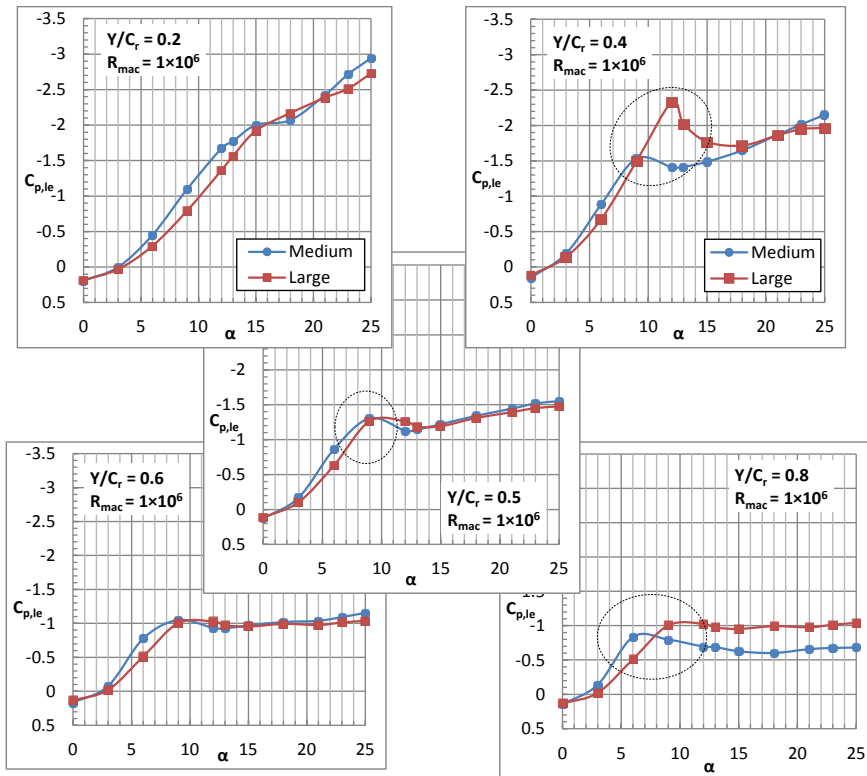


Figure 11

The bluntness effects to leading edge pressures at $R_{mac} = 1 \times 10^6$

The flow characteristics at higher Reynolds of 3×10^6 are shown in Figure 12 below. At this Reynolds number, the effects of leading edge bluntness are more obvious. At position $Y/C_r = 0.2$, the onset of the primary vortex is developed at $\alpha = 12^\circ$ for medium-edged wing, while for the large-edged wing, the primary vortex is still not developed even when the attack angle has been increased to $\alpha = 21^\circ$. At position $Y/C_r = 0.4$, it can be seen that the primary vortex has developed at $\alpha = 9^\circ$ for the medium-edged wing, while it developed at a higher attack angle of $\alpha = 18^\circ$ on the blunter wing. A similar situation happened at Y/C_r of 0.5, 0.6 and 0.8. The current data here showed that the upstream progression of the primary vortex has been delayed if the leading edge bluntness is increased [24].

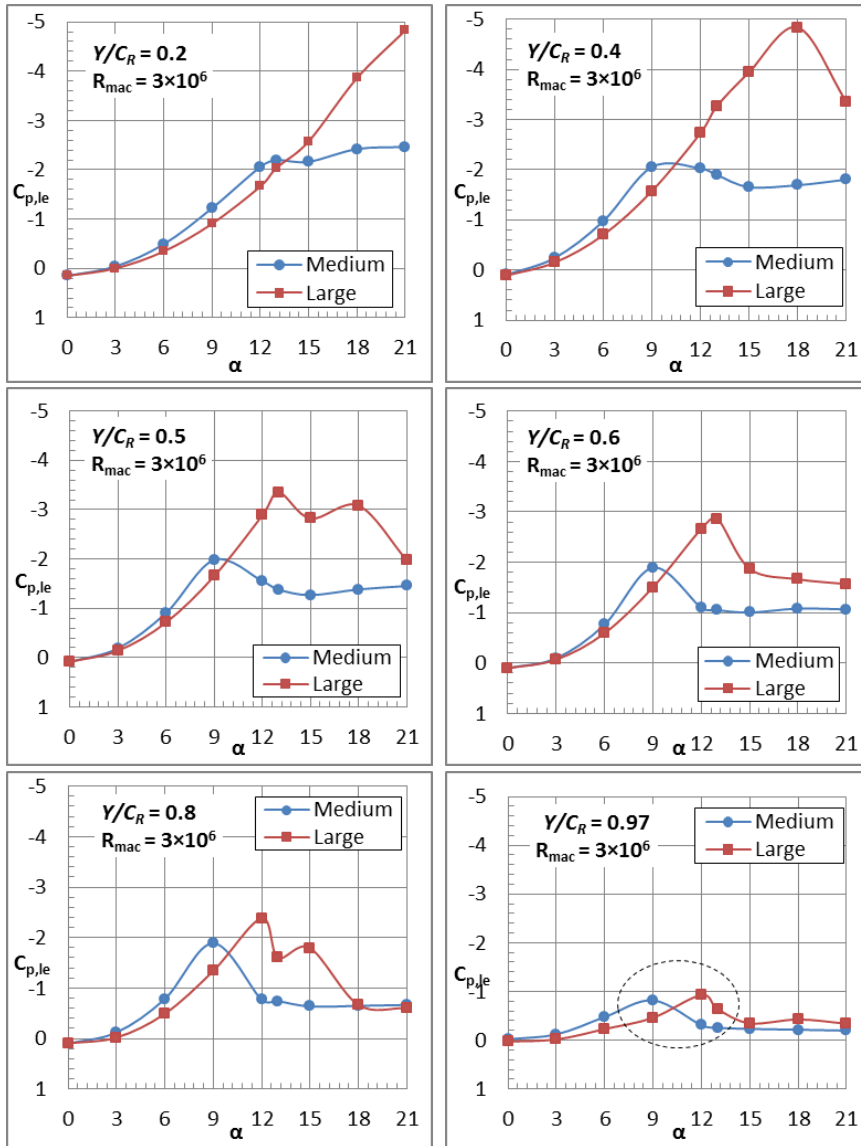


Figure 12
The bluntness effects to leading edge pressures at $R_{mac} = 3 \times 10^6$

3.2 Reynolds Number Effects on Large-edged Wing

Since the data on large-edged wing is limited, this section will further discuss the effects of Reynolds number, angle of attack on this wing. The effects of Reynolds

number at constant angle of attack of $\alpha = 13^\circ$ is presented in Figure 13 below. The data compared the surface pressure on the upper surface at three different Reynolds numbers of 1×10^6 , 2×10^6 and 3×10^6 . The primary vortex developed at about a 20% chordwise distance from the apex ($Y/C_r = 0.2$) at a Reynolds number of 1×10^6 . When the Reynolds number is increased to 2×10^6 and 3×10^6 , the primary vortex shifted further aft of the wing to at about $Y/C_r = 0.4$ and $Y/C_r = 0.6$ of the apex. The results showed that the increase in Reynolds number has slowed down the primary vortex further aft of the wing. The results here were consistent with [13].

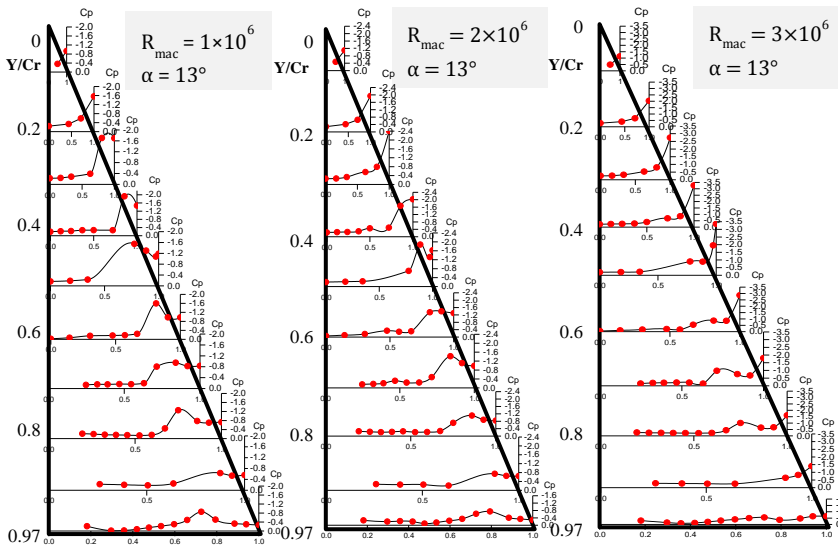


Figure 13

Reynolds number effects on large-edged wing at $\alpha = 13^\circ$

The flow characteristics when the angle of attack is increased to $\alpha = 18^\circ$ is shown in Figure 14. Similar flow physics is observed here where the Reynolds number has delaying the upstream progression of the primary vortex further aft of the wing. The surface flow topology in the second figure showed the primary vortex has been shifted more outboard when the Reynolds number is increased. In addition, the magnitude of pressure topology formed in the leading increases when the Reynolds number is increased. This shows that the primary vortex is stronger when the Reynolds number is increased. The plot of surface pressure in the third figure at Y/C_r at 0.7 also showed that the primary vortex is shifted outboard with the Reynolds number. The characteristics of the flow either being laminar or turbulence, the main factor that leads to these results [6]. At a low Reynolds number where the flow is dominated by laminar flow, the onset of the primary vortex develops earlier. The stronger ability of the turbulent boundary layer at higher Reynolds number has endured the adverse pressure gradient and thus delaying the development of the primary vortex [6, 15].

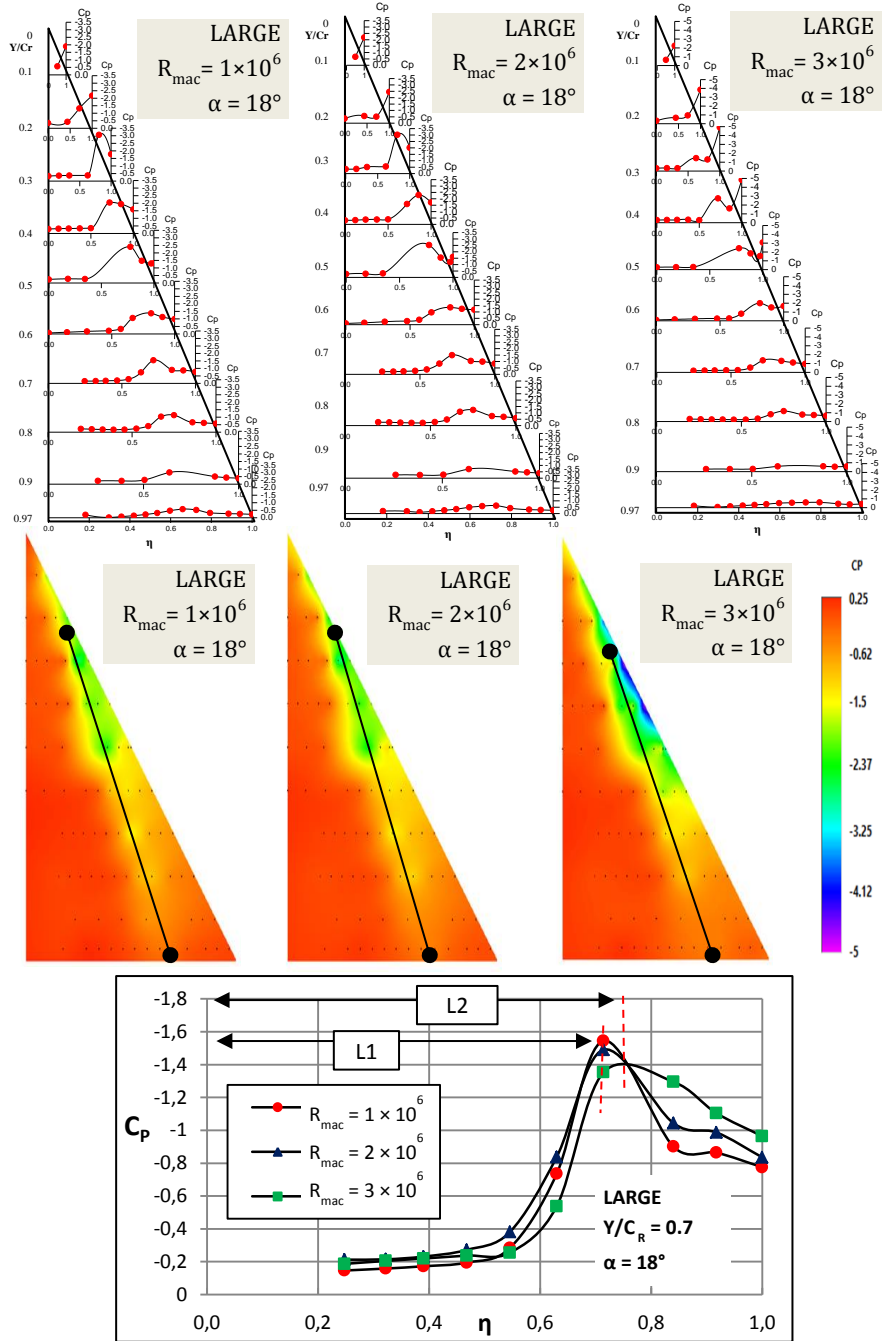


Figure 14

Reynolds number effects on large-edged wing at $\alpha = 18^\circ$

One of the problems that cannot be solved with the VFE-2 for medium-edged wings was to assess the laminar/turbulent status. At lower Reynolds number the flow is laminar and it is turbulent at high Reynolds number, S. Mat [13] in his experiment has shown that the flow at Reynolds number 1×10^6 is dominated by laminar flow. The Figure 15 shows the distribution of pressure coefficients at Reynolds number of 1×10^6 for the large-edged wing. From the figure, it can be observed that the flow is attached to the surface at relatively low attack angles. In addition, it can be noted also that the attached flow still existed even if the attack angle of attack has been increased to $\alpha = 23^\circ$. The boundary layer status is still unverified from this experiment. More experiments are needed to verify this.

4 Further Experiments on Blunt-edged Delta Wing

Delta wing is the best platform for the development of the Unmanned Air Combat Air Vehicle (UACV) aircraft. For most UCAV aircrafts, the wing has been designed with blunt leading edge. The data obtained from this experiment provides a useful knowledge for future UCAV development. In a continuation of the VFE-2 project, another model of delta derivative wing called diamond wing was proposed and is currently fabricated. The interests in this project were an extended research project that initiated from AVT-183 task group, a collaborative task group with AVT-113 under NATO. This research project will focus on understanding the detail interactions between the inboard inner vortex and the primary vortex of blunt-leading-edged vortex separation. The diamond wing was configured with blunt leading-edge of constant airfoil, moderate leading-edge sweep of 53° categorized as non-slender wing, and swept trailing edge as shown in Figure 16.

Besides the ability to induce vortex potential lift, diamond wing configurations with blunt and reduced sweep angle were more relevant to application because it also can enhance aircraft longitudinal static stability [25]. However, diamond wings exhibit more complex vortical flows as compared to slender, sharp-edged wings. The vortices formed on diamond wings are more unsteady and breakdown occurs at a much lower angle of attack than on highly-swept slender wings.

This current research was focused to investigate the inboard inner vortex effects to the onset and progression of leading-edge vortex separation. The leading-edge vortices investigation will have both moderate-sweep effects and blunt-leading-edge effects, coupled together [26]. Several measurement techniques will be employed on the wing suitable to measure the unsteady vortices on the diamond wing configuration as shown in Figure 17.

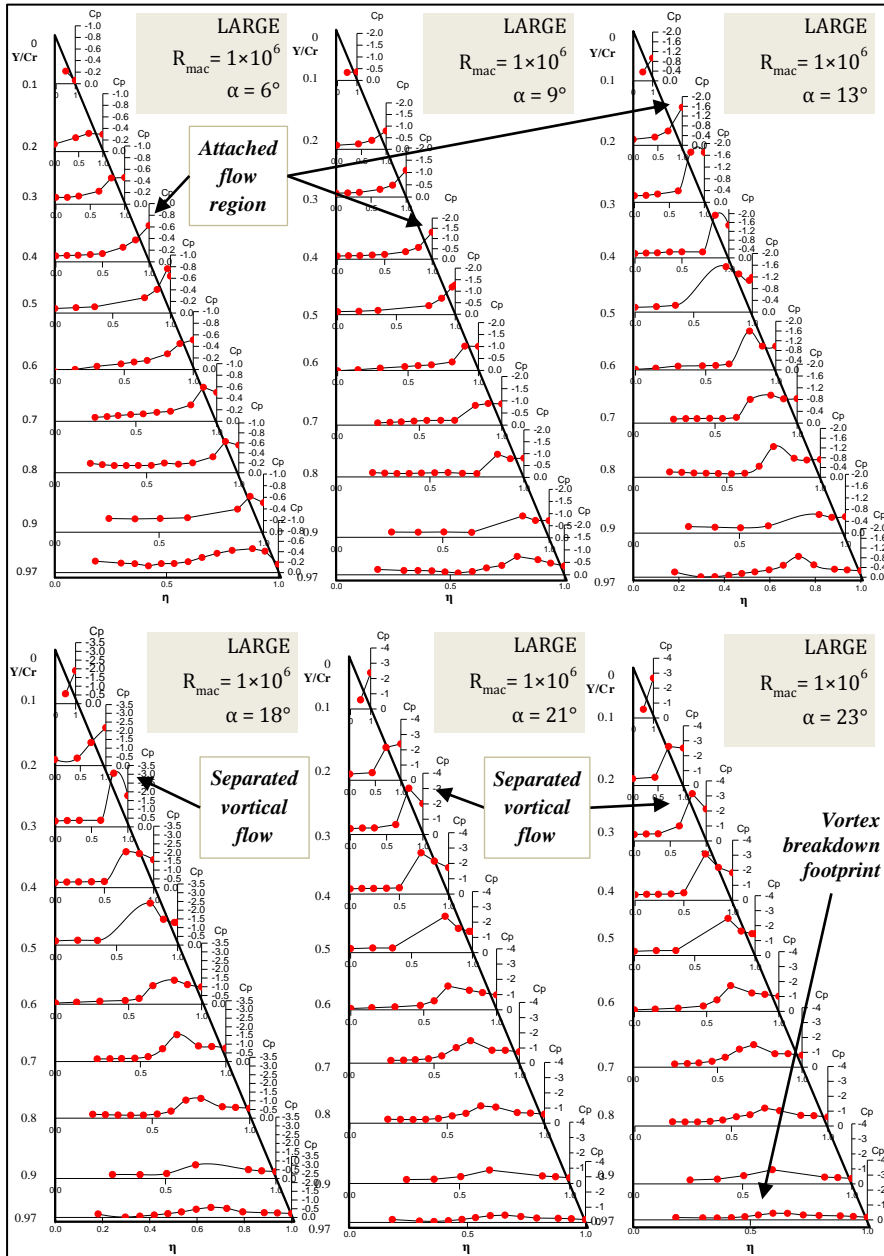


Figure 15

Pressure distribution on large-edge wing at $R_{mac} = 1 \times 10^6$ at various angles of attack

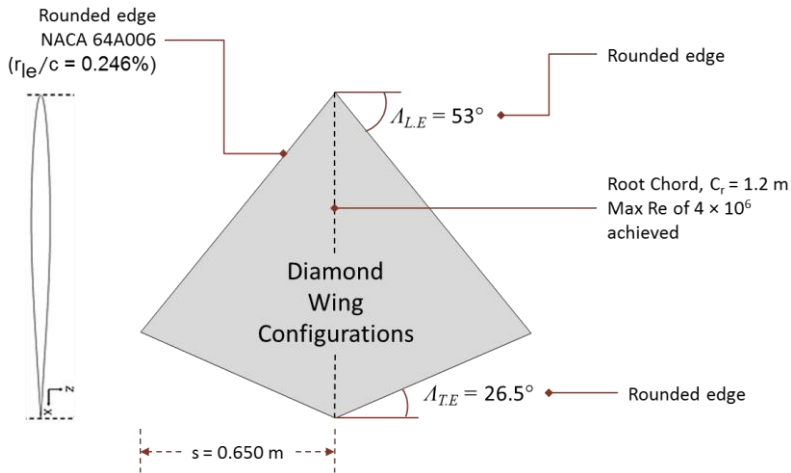


Figure 16
Diamond wing configurations

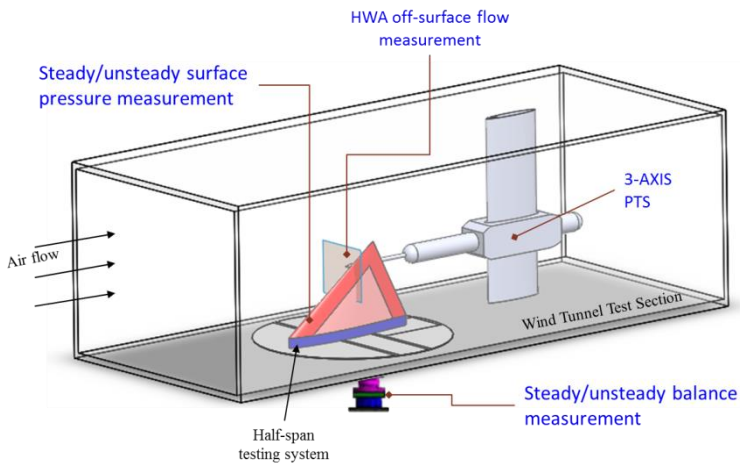


Figure 17
UTM Diamond wing experimental setup and measurements

Conclusions

This paper discusses further the effects of leading edge bluntness on the vortex properties above blunt-edged delta wing. In the VFE-2 campaign, concentrations have been given to a medium-edged wing. A series of experiments were conducted to study the performance of vortex on the blunter wing of large-edged wing. The results obtained from the large-edged wing have been compared with those from the medium-edge wing. The current results here showed that the primary vortex above large-edged delta wing is also dependent on Reynolds

number, leading edge bluntness and angle of attack. The results from steady balance data has showed that the lift/drag ratio is increased if the leading edge bluntness increases. Among the important observations from this study was the area covered by attached flow is enlarged. That the primary vortex also developed further aft of the wing has been shifted outboard to the leading edge area with the bluntness effects. The advantage of the blunter wing also that the formation of the vortex breakdown and its upstream progression has been delayed. Since most of the UCAV aircrafts are in the delta-shaped planform, this paper has highlighted some of the most important considerations in the design stage such as the progression of the primary vortex and vortex breakdown behaviors.

Acknowledgement

This research was funded by a grant from Ministry of Higher Education Malaysia (UTM Research University Grant No. 4F172, 4F718 and 12H06). The data presented, the statement made, and views expressed are solely the responsibility of the author.

References

- [1] Kulfan, R. M. (1979) Wing Geometry Effects on Leading Edge Vortices. Aircraft Systems and Technology Meeting. 20-22 August. New York, 79 – 1872
- [2] Earnshaw, P. B. (1962) An Experimental Investigation of the Structure of a Leading- Edge Vortex. Aeronautical Research Council Reports and Memoranda, No 3281
- [3] Pershing, B. (1964) Separated Flow Past Slender Delta Wings With Secondary Vortex Simulation. El Segundo Technical Operations. TDR–269(4560 – 10) – 4
- [4] Gad-El-Hak, M. and Blackwelder, R. F. (1985) The discrete Vortices from a Delta Wing. Technical Report 1985, Vol. 23, 961-962
- [5] Hummel, D. (1979) On the vortex formation over a slender wing at large incidence. AGARD-CP-247, Paper No. 15
- [6] Hummel, D. (2004) Effects of Boundary layer Formation on the vortical Flow above Slender Delta Wings. RTO specialist Meeting on Enhancement of NATO military Flight Vehicle Performance by Management of Interacting Boundary Layer transition and Separation. Meeting Proceedings RTO-MPAVT- 111. Page 30-1 to 30-2
- [7] Luckring, J. M. (2004a) Compressibility and Leading-Edge Bluntness Effects for a 65° Delta Wing. 42th AIAA Aerospace Science Meeting and Exhibit. 5-8 January, Reno, Nevada. AIAA-2004-0765
- [8] Luckring, J. M. (2004b) Reynolds Number, Compressibility, and Leading Edge Bluntness Effects on Delta Wing Aerodynamics. 24th International

- Congress of the Aeronautical Sciences. 29 – 3 September. Yokohama, Japan
- [9] Luckring, J. M. (2013) Initial Experiments and Analysis of Blunt-edge Vortex Flows for VFE-2 configurations at NASA Langley, USA. *Aerospace Science and Technology*. Vol. 24, Issue 1, pp. 10-21
- [10] Chu, J. and Luckring, J. M. (1996) Experimental Surface Pressure Data Obtained on 650 Delta Wing across Reynolds Number and Mach number Ranges. NASA Technical Memorandum 4645
- [11] Coton, F., Mat, S. B., and Galbraith, R. (2008) Chapter 22 – Experimental Investigations on the VFE-2 Configuration at Glasgow University, United Kingdom. RTO-TR-AVT-113, Pages 22-1 – 22-18
- [12] Mat, S. B., (2011) The analysis of flow on round-edged delta wings. Doctor Philosophy. University Of Glasgow, United Kingdom
- [13] Mat, S. B., Green, R., Galbraith, R., and Coton, F. (2015) The Effect of Edge Profile on Delta Wing Flow. Proceedings of the Institution of Mechanical Engineers, Part G: Journal of Aerospace Engineering
- [14] Kurun, S. (2008) Chapter 23 – Experimental Investigations on the VFE-2 Configuration at TUBITAK-SAGE, TURKEY. RTO-TR-AVT-113. Pages 23-1 – 23-18
- [15] Furman, A. and Breitsamter, C. (2013) Turbulent and Unsteady Flow Characteristics of Delta Wing Vortex Systems. *Aerospace Science and Technology*. Vol. 24, Issue 1, pp. 32-44
- [16] Rodriguez, O. (2008) Chapter 20 – Experimental Investigation on the VFE-2 Configuration at ONERA, France. RTO-TR-AVT-113
- [17] Luckring, J. M. and Hummel, D. (2008) Chapter 24 – What Was Learned From The New VFE-2 Experiments. RTO-TR-AVT-113
- [18] Luckring, J. M. and Hummel, D. (2013) What Was Learned From The New VFE-2 Experiments. *Aerospace Science and Technology*. Vol. 24, Issue 1, pp. 77-88
- [19] Tajuddin, N., Mat, S., Said, M. and Mansor, S. (2017) Flow Characteristic of Blunt-edged Delta Wing at High Angle of Attack. *Journal of Advanced Research in Fluid Mechanics and Thermal Sciences*. Vol. 39. Issue 1, pp. 17-25
- [20] Konrath, R., Klein, C., and Schröder, A. (2013) PSP and PIV Investigation on the VFE-2 Configuration in Sub- and Transonic Flow. *Aerospace Science and Technology*. Vol. 24, Issue 1, pp. 22-31
- [21] Ronoie, K. (1996) Low Speed Aerodynamics Characteristics of 60° Rounded Leading-Edge Delta Wing with Vortex Flaps: Part 1: 457 mm Span Delta Wing. Cranfield University. COA Report No. 9611

- [22] Said, M. B., (2016) Effects of Leading Edge Radius, Reynolds number and Angle of Attack on The Vortex Formation above Large-Edged Delta Wing. Master Degree. Universiti Teknologi Malaysia, Malaysia
- [23] Renac, F., Barberis, D. and Molton, P. (2005) Control of Vortical Flow over a Rounded Leading- Edge Delta Wing. *AIAA Journal*. Vol. 43, No. 7, pp. 1409-1417
- [24] Said, M. and Mat, S., (2016) Effects of Reynolds Number on The Onset of Leading Edge Vortex Separation Above Blunt-edge Delta Wing VFE-2 Configurations. 30th Congress of the International Council of the Aeronautical Sciences, 25-30 September, Daejeon, South Korea, 2016_0608
- [25] Hitzel, S. M. (2013) Perform and Survive – Evolution of Some U(M)CAV Platform Requirements. STO AVT Workshop on Innovative Control Effectors for Military Vehicles. Stockholm, Sweden, 20-22 May, No. 1, STO-MP-AVT-215
- [26] Luckring, J. M, Boelens, O. J., Breitsamter, C., Hövelmann, A., Knoth, F., Malloy, D. J., Decke, S. (2016) Objectives, approach, and scope for the AVT-183 diamond-wing investigations. *Aerospace Science and Technology*. Vol. 57, pp. 2-17